

From Majority to Minority: A Diffusion-based Augmentation for Underrepresented Groups in Skin Lesion Analysis

Janet Wang, Yunsung Chung, Zhengming Ding, and Jihun Hamm

Tulane University
{swang47, ychung3, zding1, jhamm3@tulane.edu}

Abstract. AI-based diagnoses have demonstrated dermatologist-level performance in classifying skin cancer. However, such systems are prone to under-performing when tested on data from minority groups that lack sufficient representation in the training sets. Although data collection and annotation offer the best means for promoting minority groups, these processes are costly and time-consuming. Prior works have suggested that data from majority groups may serve as a valuable information source to supplement the training of diagnosis tools for minority groups. In this work, we propose an effective diffusion-based augmentation framework that maximizes the use of rich information from majority groups to benefit minority groups. Using groups with different skin types as a case study, our results show that the proposed framework can generate synthetic images that improve diagnostic results for the minority groups, even when there is little or no reference data from these target groups. The practical value of our work is evident in medical imaging analysis, where under-diagnosis persists as a problem for certain groups due to insufficient representation.

Keywords: Skin Lesion Analysis · Diffusion Models · Data Augmentation.

1 Introduction

Current AI-assisted diagnostic systems demonstrate expert-level capability in classifying skin cancers, often identified visually. [6,16,2]. These systems can potentially contribute to teledermatology as diagnostic and decision-support tools, enhancing diagnostic accessibility in rural areas [3]. However, despite such success, recent studies have highlighted their susceptibility to under-diagnosing minority groups, such as those with underrepresented skin types, hindering their ability to generalize across different demographic groups [4,11]. Although the majority group contains rich lesion information, directly training models for cross-color classification using this data is challenging due to the domain gap caused by varying skin types [24]. Prior research has suggested using synthetic images generated from majority groups to supplement the training for minority groups [19].

Augmenting skin condition data with synthetic images has been explored, owing to its potential to address common challenges for skin lesion analysis, such as data privacy, imbalance, and scarcity. Notably, Generative Adversarial Networks (GANs) [10] and Diffusion Models (DMs) [5] have emerged as leading techniques for generating high-quality skin lesion images. While GANs have successfully produced photorealistic synthetic images, their generation is uncontrollable [9,18]. On the other hand, DMs pre-trained on extensive web data have enabled higher controllability over image generation through the guidance of textual prompts, allowing for the creation of diverse and high-fidelity images of target skin conditions and types.

Existing studies have used diffusion models to augment skin disease datasets and improve diagnosis for minority skin types using two public datasets: Diverse Dermatology Images (DDI) [4] and Fitzpatrick17k [11]. Each image in these datasets is annotated with skin type labels based on the Fitzpatrick scoring system [7]. In their work, [21] generated multiple synthetic images for each real image using Stable Diffusion [20] and then trained the classifier on a dataset including real and synthetic data. They find that diffusion models can enhance classifier performance across skin types in binary malignancy classification on the DDI dataset, though the number of real images remains a key driver in performance. Additionally, [22] sampled a small number of seed images with skin type at the end of the Fitzpatrick spectrum (FST I-II and FST V-VI) and carefully cropped the disease pathology, before generating synthetic data from the seed data with OpenAI DALL·E 2’s inpainting feature. They conducted class-wise data augmentation by incorporating synthetic images of the target condition and minority skin type into the real training set. Other related studies have focused on internal datasets [1,15].

Despite these advancements, the potential to leverage diffusion models’ knowledge about skin variation and the rich lesion information from majority groups to benefit minority groups remains underexplored. In this work, we propose a novel diffusion-based augmentation framework capable of learning skin lesion concepts from majority groups and generating images to improve classification performance for minority groups. Unlike current works that assume the existence of data from minority groups, we hypothesize that the information gained from majority groups and the diffusion model’s knowledge is sufficient to generate useful synthetic data. We test our hypothesis in a challenging multi-condition task. The framework is illustrated in Fig. 1. We conduct our experiments on the Fitzpatrick17k dataset, which includes lesions that are less familiar to diffusion models than common skin cancer. This dataset has a skewed skin type distribution, with light skin types (FST I-II) being significantly more common than dark skin types (FST V-VI), thus forming majority and minority groups. Our investigation focuses on images from both groups and is structured around three scenarios with increasing difficulty: **(i)** the training source includes some data from both groups; **(ii)** there is limited data from the minority group in the training source; and **(iii)** the training source lacks data from the minority group. Our findings reveal:

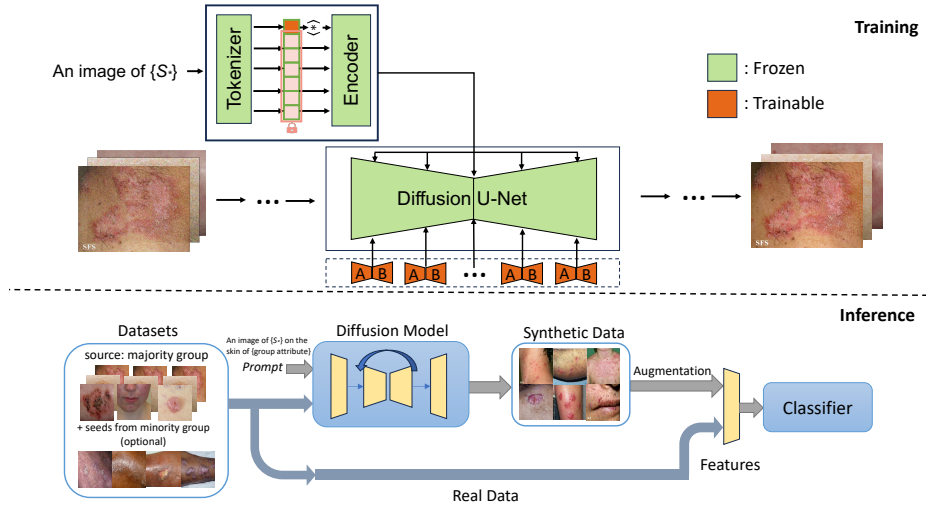


Fig. 1. Outline of the proposed augmentation framework. The framework pairs each training image with a textual prompt describing the condition as an input to train a latent diffusion model. Embeddings associated with new lesion concepts are found through Textual Inversion. Compact matrices A and B are optimized with LoRA to facilitate training with the new embeddings. During inference, the trained model produces synthetic images from the training data that mainly feature the majority groups via image-to-image generation, thus conditioned on visual cues of lesions from images and textual prompts describing the target condition and group attributes.

- Our proposed method effectively leverages lesion information from the majority group to generate synthetic images that can improve classification results for the minority group across all settings, even without reference data from the minority group.
- Using synthetic images generated by our method to train classifiers consistently outperforms training with only real images across various architectures. Further improvement is observed when combining real and synthetic data.
- Our method is sensitive to information from the minority group. A notable improvement can be observed when even a few examples from the minority group are added to the training set.

2 Methods

2.1 Latent Diffusion Models

We implement our method using Latent Diffusion Models (LDMs) [20], a class of Denoising Diffusion Probabilistic Models (DDPMs) [13] that operate in the latent space of an autoencoder, to enable DDPM training with limited computational resources. LDMs include two core components: a pre-trained autoencoder and a diffusion model. In our study, the encoder of the autoencoder

<i>FST</i>	Basal Cell Carcinoma	Folliculitis	Nematode Infection	Neutrophilic Dermatoses	Prurigo Nodularis	Psoriasis	Squamous Cell Carcinoma	<i>Total</i>
<i>I</i>	85	30	15	70	7	113	100	420
<i>II</i>	156	97	56	115	28	232	180	864
<i>V</i>	24	31	32	31	29	64	40	251
<i>VI</i>	7	9	12	15	9	21	23	96
Total	272	167	115	231	73	430	343	1631

Table 1. Sample distribution across skin conditions by Fitzpatrick Skin Type.

\mathcal{E} encodes skin lesion images $x \in \mathcal{D}_x$ into a latent representation $z = \mathcal{E}(x)$, while the decoder D maps the latent representations back to images, such that $D(\mathcal{E}(x)) \approx x$. The diffusion model is trained to generate representations conditioned on prompts describing skin disease and skin type, within the learned latent space. Let $c_\theta(y)$ be a model that maps a conditioning input y into a vector. We then learn the conditional LDM via

$$L_{LDM} := \mathbb{E}_{z \in \mathcal{E}(x), y, \epsilon \in \mathcal{N}(0,1), t} \left[\|\epsilon - \epsilon_\theta(z_t, t, c_\theta(y))\|_2^2 \right], \quad (1)$$

where t is the time step, z_t is the latent noise at time t , ϵ is the unscaled noise sample, and ϵ_θ is the denoising network.

2.2 Concept Discovery via Textual Inversion

Our proposed framework leverages Textual Inversion [8] to capture a unique embedding that accurately represents the targeted skin lesion concept from training data. Skin lesion images paired with a string containing a placeholder word (e.g., ‘An image of $\{S_*\}$ ’) are used to guide the learning of new lesion embedding for the generative model. In particular, The optimal embedding v_* for the lesion concept S_* is derived by minimizing the reconstruction loss

$$v_* = \operatorname{argmin}_v \mathbb{E}_{z \sim \mathcal{E}(x), y, \epsilon \in \mathcal{N}(0,1), t} \left[\|\epsilon - \epsilon_\theta(z_t, t, c_\theta(y))\|_2^2 \right]. \quad (2)$$

This objective encourages the embedded representation to encapsulate new concepts specialized to skin disease datasets by re-using the same training scheme as the original LDM model while keeping both c_θ and ϵ_θ fixed.

2.3 Fine-grained Detail Enhancement with LoRA

To enhance efficiency in fine-tuning LDM, we employ Low-Rank Adaptation (LoRA) [14] in our framework, with the discovered tokens after textual inversion. This fine-tuning strategy freezes the pre-trained model weights and introduces two compact matrices A and B , where $A \in \mathbb{R}^{n \times r}$, $B \in \mathbb{R}^{r \times n}$. The adaptation matrices AB are integrated into the attention layers to capture the fine visual details of the skin lesion concept with target embedding v_* . The optimization is formulated as

$$L := \mathbb{E}_{z \sim \mathcal{E}(x), y, \epsilon \in \mathcal{N}(0,1), t} \left[\|\epsilon - \epsilon_{\theta_{AB}}(z_t, t, c_{\theta_{AB}}(v_*))\|_2^2 \right]. \quad (3)$$

This step further strengthens the model to generate synthetic images that reflect fine-grained features not initially present in the pre-trained model.

Architecture	Train	Accuracy	Precision	Recall	F1 Score
VGG-16	real	70.24 ± 0.12	72.49 ± 0.37	69.58 ± 0.30	70.48 ± 0.13
	syn	75.00 ± 0.64	75.77 ± 0.39	73.17 ± 0.29	72.42 ± 0.61
	real + syn	77.98 ± 0.40	81.51 ± 0.25	78.87 ± 0.23	77.45 ± 0.29
ResNet-18	real	68.45 ± 0.42	69.42 ± 0.57	69.05 ± 0.42	67.94 ± 0.35
	syn	69.05 ± 0.36	69.57 ± 0.82	69.05 ± 0.42	68.02 ± 0.33
	real + syn	71.36 ± 0.69	69.02 ± 0.48	68.45 ± 0.40	67.56 ± 0.59
ViT-B-16	real	70.38 ± 0.42	73.72 ± 0.69	70.82 ± 0.39	70.61 ± 0.59
	syn	74.19 ± 0.37	77.89 ± 1.01	74.04 ± 0.85	73.58 ± 0.53
	real + syn	78.65 ± 0.53	81.57 ± 0.47	79.17 ± 0.84	78.24 ± 0.64

Table 2. This table presents the results when the training set includes some (291 non-seed) images from the minority group. The test set comprises 56 seed images of the minority group (FST V-VI), uniformly distributed across the 7 conditions. Here, “real” indicates that the classifier is trained solely on real images, while “syn” means that it is trained exclusively on synthetic images generated by our framework. Accordingly, “real+syn” means that the subsequent classifier is trained on a combination of both.

3 Experiments

We conduct our experiments using the Fitzpatrick17k dataset, where each image is annotated with a condition and a Fitzpatrick Skin Type (FST) label. In line with [22], our analysis narrows down to a subset of the Fitzpatrick17k dataset, encompassing 7 conditions (Table 1). These conditions were selected because they represent the largest sample sizes at the ends of the Fitzpatrick Skin Type (FST I-II or V-VI) spectrum. Unlike [22], our study excludes intermediate skin types (FST III-IV), to explore the efficacy of our diffusion-based augmentation in a more challenging and explainable way. For each condition, we randomly sample 8 images from the lightest (FST I-II) and darkest (FST V-VI) skin type groups, resulting in 56 seed images for each group.

We independently examine three scenarios: **(i)** the training source includes some images of both dark and light skin types, and the target features uniformly distributed seed images (56 of one skin type) over the 7 conditions; **(ii)** there are many light-skinned images and a few dark-skinned seed images in the training set. In this setting, the target consists of 291 holdout images of dark skin type; and **(iii)** the source lacks dark-skinned images entirely and includes only light skin type. Likewise, the target comprises of 291 dark-skinned images. In all the settings, we generate 5 synthetic images for each real one in the source training set during inference, using the fine-tuned model, as illustrated by Fig. 1.

In setting **(i)**, to ensure a sufficient number of examples for both majority and minority groups (lightest vs. darkest skin types), we designate the seed images as the target and utilize all remaining images as sources for generator and classifier training. Meanwhile, this setting also serves as the basis for hyperparameter tuning of the diffusion model, with the chosen hyperparameters being fixed for subsequent experiments. In setting **(ii)**, we reversed the roles of the seed and non-seed images, creating a training set composed of 56 dark-skinned

Architecture	Train	Accuracy	Precision	Recall	F1 Score
VGG-16	real	58.79 ± 0.10	58.90 ± 0.03	58.26 ± 0.05	56.98 ± 0.04
	syn	62.86 ± 0.15	61.49 ± 0.15	63.32 ± 0.13	61.57 ± 0.24
	real + syn	63.66 ± 0.11	62.80 ± 0.12	64.08 ± 0.08	62.72 ± 0.18
ResNet-18	real	50.31 ± 0.30	50.45 ± 0.44	51.27 ± 0.30	48.23 ± 0.32
	syn	56.36 ± 0.16	56.58 ± 0.13	59.78 ± 0.08	55.58 ± 0.10
	real + syn	61.33 ± 0.17	59.75 ± 0.12	62.52 ± 0.17	59.94 ± 0.17
ViT-B-16	real	62.03 ± 0.19	63.09 ± 0.13	62.02 ± 0.04	61.05 ± 0.04
	syn	68.83 ± 0.19	70.07 ± 0.03	68.22 ± 0.25	68.34 ± 0.19
	real + syn	71.20 ± 0.07	71.61 ± 0.19	71.53 ± 0.01	71.17 ± 0.13

Table 3. Classification results when the training set contains few reference images from the minority group (56). The test set has 291 non-seed images of the minority group (FST V-VI).

seed images with other light-skinned ones, and a test set of 291 dark-skinned images. In the final setting, we removed the seed images from the training set to evaluate whether our pipeline could still generate synthetic images that enhance classification performance for the target minority groups, even without any visual references from them. Note that the same set of images is used for training the diffusion model and classifier in all settings.

Implementation Details In each setting, we sampled 5 groups of seed images and repeated the experiment 5 times. We used the Stable Diffusion 2.1 base [20] and the Diffusers library [17] for fine-tuning the diffusion model and generating synthetic images. We used pre-trained VGG-16 [23], ResNet-18 [12], and ViT-B-16 [25] as classifier backbones and trained each classifier for 30 epochs using the Adam optimizer with an initial learning rate of 1e-3. A weight-based sampler and StepLR scheduler were applied. Experiments were conducted on two NVIDIA GeForce RTX 3090s.

4 Results

To assess the efficacy of our augmentation framework across the three settings, we train the classifier on data that includes real images only, synthetic images only, or a combination of both, respectively. Our evaluation is based on four metrics: accuracy, precision, recall, and F1. First, in the setting with some images from both majority and minority groups in the training set, we observe that synthetic data enhances performance across all architectures (Table 2). Specifically, classifiers trained on synthetic images consistently outperform those trained solely on real ones, and the combination of both types of data for training yields further improvements.

This trend of consistent improvement is also evident in the more challenging scenarios where there are little or no reference images from the minority groups (Tables 3 and 4) in the training set. Notably, significant improvement is observed when just a few reference images from the minority group are available in the

Architecture	Train	Accuracy	Precision	Recall	F1 Score
VGG-16	real	55.58 \pm 0.10	54.60 \pm 0.11	51.84 \pm 0.29	51.97 \pm 0.45
	syn	57.62 \pm 0.09	56.62 \pm 0.15	55.42 \pm 0.20	55.36 \pm 0.22
	real + syn	58.08 \pm 0.08	57.36 \pm 0.13	55.78 \pm 0.17	55.85 \pm 0.23
ResNet-18	real	49.42 \pm 0.36	49.79 \pm 0.44	48.30 \pm 0.23	47.42 \pm 0.30
	syn	53.47 \pm 0.32	52.39 \pm 0.30	53.79 \pm 0.30	51.97 \pm 0.29
	real + syn	56.50 \pm 0.15	55.72 \pm 0.15	55.10 \pm 0.16	54.76 \pm 0.18
ViT-B-16	real	57.66 \pm 0.35	61.89 \pm 0.68	55.45 \pm 0.36	55.96 \pm 0.51
	syn	58.94 \pm 0.23	62.79 \pm 0.20	55.62 \pm 0.22	56.53 \pm 0.18
	real + syn	60.96 \pm 0.31	64.57 \pm 0.01	57.51 \pm 0.29	58.92 \pm 0.31

Table 4. Classification results when no image from the minority group is in the training set. The test set has 291 non-seed images of the minority group (FST V-VI).

training set for image generation and classification. The transformer-based classifier demonstrates a larger improvement gap over the real image baseline than the CNN-based models. In the most challenging setting, with no reference images from the minority group, the improvement margin narrowed, suggesting our pipeline effectively maximizes the use of limited information from the seed images of the minority groups in the training process. Despite these challenges, the sustained improvements in the third setting validate our framework’s effectiveness in transferring information across groups. Examples of real and synthetic image pairs for each condition are presented in Fig. 2. Qualitatively, the synthetic images generated by our augmentation framework introduce more diversity to the training sets, including variations in skin color and lesion patterns.

To further investigate our framework’s generation capabilities, we conduct an ablation study comparing our framework with various generation strategies. This study focuses on the first setting, where the test set consists of light- or dark-skinned seed images (56 for each type). We first examine the Stable Diffusion’s vanilla text-to-image and image-to-image pipelines to generate synthetic images. Next, we leverage Textual Inversion to learn the lesion embeddings and generate synthetic images from these embeddings, with text-to-image and image-to-image pipelines. Since image-to-image outperforms text-to-image in both vanilla SD and Textual Inversion generation, we focus on image-to-image generation after fine-tuning the diffusion model using LoRA, to investigate if optimizing the diffusion model can benefit the generation even more. We train a VGG-16 using only the synthetic images and then compare these generation strategies with ours, as shown in Table 5.

Overall, training classifiers on synthetic images generated by text-to-image models proves less effective than employing image-to-image techniques, underscoring the importance of visual cues in augmenting skin lesion classification. Additionally, using off-the-shelf models for image generation yields less improvement than utilizing training strategies such as Textual Inversion and LoRA, regardless of whether the target is a minority or majority group. Finally, the combination of Textual Inversion and LoRA results in the highest accuracy, thereby

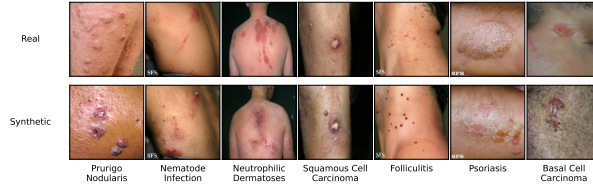


Fig. 2. Examples of real and synthetic image pairs. Synthetic images were generated by a model trained on light-skinned images only, using prompts conditioned on dark skin types.

validating the practicality of our design which integrates these two strategies. This improvement can be explained by the model’s enhanced ability to associate the fine visual cues of the lesion with the learned textual tokens.

Since a direct comparison with existing related works is challenging due to the uncertain use of data, this ablation study can serve as an indirect comparison. As introduced previously, related works either leveraged off-the-shelf diffusion models such as DALL·E or fine-tuned a Stable Diffusion model for text-to-image generation. Our results demonstrate that utilizing the dual guidance of visual cues and text via fine-tuning diffusion models can maximize the potential of diffusion-based augmentation to enhance the diagnosis for minority groups.

target	txt2img		img2img			
	vanilla	ti	vanilla	ti	lora	ti+lora
light (56)	18.80	35.36	48.21	46.43	52.00	53.57
dark (56)	21.22	44.64	69.64	71.43	73.21	79.57

Table 5. Classification accuracy with various generation strategies for the first setting. Here, “vanilla” stands for Stable Diffusion’s original text-to-image and image-to-image pipelines, “ti” for Textual Inversion, and “lora” for LoRA.

5 Conclusion

In this work, we present an effective diffusion-based augmentation framework that consistently improves classification results for the minority group, even when training the classifier exclusively with synthetic images. This improvement is observed regardless of the availability of reference data from the minority group in the training set. The ablation study also validates that our framework’s dual-guidance generation approach successfully learns novel lesion concepts previously unfamiliar to the diffusion models. A practical takeaway from this study is that, even in cases of extreme data scarcity, existing data and diffusion models can still provide valuable insights, maximizing information usage and achieving better performance. In the future, we plan to apply this technique to other medical datasets characterized by significant differences in group sizes. Additionally, as we used all synthetic images generated for each setting without any filtering mechanism, we also aim to investigate which types of synthetic data are useful for lesion diagnosis and how to generate them.

References

1. Akrouf, M., Gyepesi, B., Holló, P., Poór, A., Kincsó, B., Solis, S., Cirone, K., Kawahara, J., Slade, D., Abid, L., Kovács, M., Fazekas, I.: Diffusion-based data augmentation for skin disease classification: Impact across original medical datasets to fully synthetic images (2023)
2. Brinker, T., Hekler, A., Enk, A., Klode, J., Hauschild, A., Berking, C., Schilling, B., Haferkamp, S., Utikal, J., Kalle, C., Fröhling, S., Weichenthal, M.: A convolutional neural network trained with dermoscopic images performed on par with 145 dermatologists in a clinical melanoma image classification task. *European Journal of Cancer* **111**, 148–154 (03 2019). <https://doi.org/10.1016/j.ejca.2019.02.005>
3. Coustasse, A., Sarkar, R., Abodunde, B., Metzger, B.J., Slater, C.M.: Use of tele-dermatology to improve dermatological access in rural areas. *Telemedicine journal and e-health : the official journal of the American Telemedicine Association* (2019)
4. Daneshjou, R., Vodrahalli, K., Liang, W., Novoa, R.A., Jenkins, M., Rotemberg, V., Ko, J., Swetter, S.M., Bailey, E.E., Gevaert, O., Mukherjee, P., Phung, M., Yekrang, K., Fong, B., Sahasrabudhe, R., Zou, J., Chiou, A.: Disparities in dermatology ai performance on a diverse, curated clinical image set. *Science Advances* (2022)
5. Dhariwal, P., Nichol, A.: Diffusion models beat gans on image synthesis. *Advances in neural information processing systems* **34**, 8780–8794 (2021)
6. Esteva, A., Kuprel, B., Novoa, R.A., Ko, J.M., Swetter, S.M., Blau, H.M., Thrun, S.: Dermatologist-level classification of skin cancer with deep neural networks. *Nature* **542**, 115–118 (2017)
7. Fitzpatrick, T.B.: The validity and practicality of sun-reactive skin types i through vi. *Archives of dermatology* **124**(6), 869–871 (1988)
8. Gal, R., Alaluf, Y., Atzmon, Y., Patashnik, O., Bermano, A.H., Chechik, G., Cohen-or, D.: An image is worth one word: Personalizing text-to-image generation using textual inversion. In: *The Eleventh International Conference on Learning Representations* (2023), <https://openreview.net/forum?id=NAQvF08TcyG>
9. Ghorbani, A., Natarajan, V., Coz, D., Liu, Y.: DermGAN: Synthetic Generation of Clinical Skin Images with Pathology. In: Dalca, A.V., McDermott, M.B., Alsentzer, E., Finlayson, S.G., Oberst, M., Falck, F., Beaulieu-Jones, B. (eds.) *Proceedings of the Machine Learning for Health NeurIPS Workshop. Proceedings of Machine Learning Research*, vol. 116, pp. 155–170. PMLR (13 Dec 2020), <https://proceedings.mlr.press/v116/ghorbani20a.html>
10. Goodfellow, I., Pouget-Abadie, J., Mirza, M., Xu, B., Warde-Farley, D., Ozair, S., Courville, A., Bengio, Y.: Generative adversarial networks. *Communications of the ACM* **63**(11), 139–144 (2020)
11. Groh, M., Harris, C., Soenksen, L., Lau, F., Han, R., Kim, A., Koochek, A., Badri, O.: Evaluating deep neural networks trained on clinical images in dermatology with the fitzpatrick 17k dataset. In: *Proceedings of the IEEE/CVF Conference on Computer Vision and Pattern Recognition*. pp. 1820–1828 (2021)
12. He, K., Zhang, X., Ren, S., Sun, J.: Deep residual learning for image recognition. In: *Proceedings of the IEEE conference on computer vision and pattern recognition*. pp. 770–778 (2016)
13. Ho, J., Jain, A., Abbeel, P.: Denoising diffusion probabilistic models. *Advances in neural information processing systems* **33**, 6840–6851 (2020)
14. Hu, E.J., yelong shen, Wallis, P., Allen-Zhu, Z., Li, Y., Wang, S., Wang, L., Chen, W.: LoRA: Low-rank adaptation of large language models. In: *International Con-*

- ference on Learning Representations (2022), <https://openreview.net/forum?id=nZeVKeeFYf9>
15. Ktena, I., Wiles, O., Albuquerque, I., Rebuffi, S.A., Tanno, R., Roy, A.G., Azizi, S., Belgrave, D., Kohli, P., Karthikesalingam, A., Cemgil, T., Gowal, S.: Generative models improve fairness of medical classifiers under distribution shifts (2023)
 16. Liu, Y., Jain, A., Eng, C., Way, D.H., Lee, K., Bui, P., Kanada, K., de Oliveira Marinho, G., Gallegos, J., Gabriele, S., Gupta, V., Singh, N., Natarajan, V., Hofmann-Wellenhof, R., Corrado, G.S., Peng, L.H., Webster, D.R., Ai, D., Huang, S.J., Liu, Y., Dunn, R.C., Coz, D.: A deep learning system for differential diagnosis of skin diseases. *Nature Medicine* **26**(6), 900–908 (Jun 2020)
 17. von Platen, P., Patil, S., Lozhkov, A., Cuenca, P., Lambert, N., Rasul, K., Davaadorj, M., Nair, D., Paul, S., Berman, W., Xu, Y., Liu, S., Wolf, T.: Diffusers: State-of-the-art diffusion models. <https://github.com/huggingface/diffusers> (2022)
 18. Qin, Z., Liu, Z., Zhu, P., Xue, Y.: A gan-based image synthesis method for skin lesion classification. *Computer Methods and Programs in Biomedicine* **195**, 105568 (2020)
 19. Rezk, E., Eltorki, M., El-Dakhkhni, W., et al.: Improving skin color diversity in cancer detection: deep learning approach. *JMIR Dermatology* **5**(3), e39143 (2022)
 20. Rombach, R., Blattmann, A., Lorenz, D., Esser, P., Ommer, B.: High-resolution image synthesis with latent diffusion models. In: *Proceedings of the IEEE/CVF Conference on Computer Vision and Pattern Recognition (CVPR)*. pp. 10684–10695 (June 2022)
 21. Sagers, L.W., Diao, J.A., Melas-Kyriazi, L., Groh, M., Rajpurkar, P., Adamson, A.S., Rotemberg, V., Daneshjou, R., Manrai, A.K.: Augmenting medical image classifiers with synthetic data from latent diffusion models (2023)
 22. Sagers, L.W., Diao, J.A., Groh, M., Rajpurkar, P., Adamson, A., Manrai, A.K.: Improving dermatology classifiers across populations using images generated by large diffusion models. In: *NeurIPS 2022 Workshop on Synthetic Data for Empowering ML Research* (2022), <https://openreview.net/forum?id=Vzdbjtz6Tys>
 23. Simonyan, K., Zisserman, A.: Very deep convolutional networks for large-scale image recognition. *arXiv preprint arXiv:1409.1556* (2014)
 24. Wang, J., Zhang, Y., Ding, Z., Hamm, J.: Achieving reliable and fair skin lesion diagnosis via unsupervised domain adaptation. In: *Proceedings of the IEEE/CVF Conference on Computer Vision and Pattern Recognition*. pp. 5157–5166 (2024)
 25. Wu, B., Xu, C., Dai, X., Wan, A., Zhang, P., Yan, Z., Tomizuka, M., Gonzalez, J., Keutzer, K., Vajda, P.: Visual transformers: Token-based image representation and processing for computer vision (2020)